Delving into Transferable Adversarial Examples and Black-box Attacks

Yanpei Liu[*]**, Xinyun Chen**[*]
Shanghai Jiao Tong University

Chang Liu, Dawn Song
University of the California, Berkeley

Abstract

An intriguing property of deep neural networks is the existence of adversarial examples, which can transfer among different architectures. These transferable adversarial examples may severely hinder deep neural network-based applications. Previous works mostly study the transferability using small scale datasets. In this work, we are the first to conduct an extensive study of the transferability over large models and a large scale dataset, and we are also the first to study the transferability of targeted adversarial examples with their target labels. We study both *non-targeted* and *targeted* adversarial examples, and show that while transferable non-targeted adversarial examples are easy to find, targeted adversarial examples generated using existing approaches almost never transfer with their target labels. Therefore, we propose novel ensemble-based approaches to generating transferable adversarial examples. Using such approaches, we observe a large proportion of targeted adversarial examples that are able to transfer with their target labels for the first time. We also present some geometric studies to help understanding the transferable adversarial examples. Finally, we show that the adversarial examples generated using ensemble-based approaches can successfully attack Clarifai.com, which is a black-box image classification system.

1 Introduction

Recent research has demonstrated that for a deep architecture, it is easy to generate adversarial examples, which are close to the original ones but are misclassified by the deep architecture (Szegedy et al. (2013); Goodfellow et al. (2014)). The existence of such adversarial examples may have severe consequences, which hinders vision-understanding-based applications, such as autonomous driving. Most of these studies require explicit knowledge of the underlying models. It remains an open question how to efficiently find adversarial examples for a black-box model.

Several works have demonstrated that some adversarial examples generated for one model may also be misclassified by another model. Such a property is referred to as *transferability*, which can be leveraged to perform black-box attacks. This property has been exploited by constructing a substitute of the black-box model, and generating adversarial instances against the substitute to attack the black-box system (Papernot et al. (2016a;b)). However, so far, transferability is mostly examined over small datasets, such as MNIST (LeCun et al. (1998)) and CIFAR-10 (Krizhevsky & Hinton (2009)). It has yet to be better understood transferability over large scale datasets, such as ImageNet (Russakovsky et al. (2015)).

In this work, we are the first to conduct an extensive study of the transferability of different adversarial instance generation strategies applied to different state-of-the-art models trained over a large scale dataset. In particular, we study two types of adversarial examples: (1) non-targeted adversarial examples, which can be misclassified by a network, regardless of what the misclassified labels may be; and (2) targeted adversarial examples, which can be classified by a network as a target label. We examine several existing approaches searching for adversarial examples based on a single model. While non-targeted adversarial examples are more likely to transfer, we observe few targeted adversarial examples that are able to transfer with their target labels.

---

[*]Work is done while visiting UC Berkeley.

We further propose a novel strategy to generate transferable adversarial images using an ensemble of multiple models. In our evaluation, we observe that this new strategy can generate non-targeted adversarial instances with better transferability than other methods examined in this work. Also, for the first time, we observe a large proportion of targeted adversarial examples that are able to transfer with their target labels.

We study geometric properties of the models in our evaluation. In particular, we show that the gradient directions of different models are orthogonal to each other. We also show that decision boundaries of different models align well with each other, which partially illustrates why adversarial examples can transfer.

Last, we study whether generated adversarial images can attack Clarifai.com, a commercial company providing state-of-the-art image classification services. We have no knowledge about the training dataset and the types of models used by Clarifai.com; meanwhile, the label set of Clarifai.com is quite different from ImageNet's. We show that even in this case, both non-targeted and targeted adversarial images transfer to Clarifai.com. This is the first work documenting the success of generating both non-targeted and targeted adversarial examples for a black-box state-of-the-art online image classification system, whose model and training dataset are unknown to the attacker.

Contributions and organization.   We summarize our main contributions as follows:

- For ImageNet models, we show that while existing approaches are effective to generate non-targeted transferable adversarial examples (Section 3), only few targeted adversarial examples generated by existing methods can transfer (Section 4).

- We propose novel ensemble-based approaches to generate adversarial examples (Section 5). Our approaches enable a large portion of targeted adversarial examples to transfer among multiple models for the first time.

- We are the first to present that targeted adversarial examples generated for models trained on ImageNet can transfer to a black-box system, i.e., Clarifai.com, whose model, training data, and label set is unknown to us (Section 7). In particular, Clarifai.com's label set is very different from ImageNet's.

- We conduct the first analysis of geometric properties for large models trained over ImageNet (Section 6), and the results reveal several interesting findings, such as the gradient directions of different models are orthogonal to each other.

In the following, we first discuss related work, and then present the background knowledge and experiment setup in Section 2. Then we present each of our experiments and conclusions in the corresponding section as mentioned above.

Related work.   Transferability of adversarial examples was first examined by Szegedy et al. (2013), which studied the transferability (1) between different models trained over the same dataset; and (2) between the same or different model trained over disjoint subsets of a dataset; However, Szegedy et al. (2013) only studied MNIST.

The study of transferability was followed by Goodfellow et al. (2014), which attributed the phenomenon of transferability to the reason that the adversarial perturbation is highly aligned with the weight vector of the model. Again, this hypothesis was tested using MNIST and CIFAR-10 datasets. We show that this is not the case for models trained over ImageNet.

Papernot et al. (2016a;b) examined constructing a substitute model to attack a black-box target model. To train the substitute model, they developed a technique that synthesizes a training set and annotates it by querying the target model for labels. They demonstrate that using this approach, black-box attacks are feasible towards machine learning services hosted by Amazon, Google, and MetaMind. Further, Papernot et al. (2016a) studied the transferability between deep neural networks and other models such as decision tree, kNN, etc.

Our work differs from Papernot et al. (2016a;b) in three aspects. First, in these works, only the model and the training process are a black box, but the training set and the test set are controlled by the attacker; in contrast, we attack Clarifai.com, whose model, training data, training process, and even the test label set are unknown to the attacker. Second, the datasets studied in these works are small

scale, i.e., MNIST and GTSRB (Stallkamp et al. (2012)); in our work, we study the transferability over larger models and a larger dataset, i.e., ImageNet. Third, to attack black-box machine learning systems, we do not query the systems for constructing the substitute model ourselves.

In a concurrent and independent work, Moosavi-Dezfooli et al. (2016) showed the existence of a *universal perturbation* for each model, which can transfer across different images. They also show that the adversarial images generated using these universal perturbations can transfer across different models on ImageNet. However, they only examine the non-targeted transferability, while our work studies both non-targeted and targeted transferability over ImageNet.

2 ADVERSARIAL DEEP LEARNING AND TRANSFERABILITY

2.1 THE ADVERSARIAL DEEP LEARNING PROBLEM

We assume a classifier $f_\theta(x)$ outputs a category (or a label) as the prediction. Given an original image x, with ground truth label y, the adversarial deep learning problem is to seek for *adversarial examples* for the classifier $f_\theta(x)$. Specifically, we consider two classes of adversarial examples. A *non-targeted* adversarial example $x^\star$ is an instance that is close to x, in which case $x^\star$ should have the same ground truth as x, while $f_\theta(x^\star) \neq y$. For the problem to be non-trivial, we assume $f_\theta(x) = y$ without loss of generality. A *targeted* adversarial example $x^\star$ is close to x and satisfies $f_\theta(x^\star) = y^\star$, where $y^\star$ is a target label specified by the adversary, and $y^\star \neq y$.

2.2 APPROACHES FOR GENERATING ADVERSARIAL EXAMPLES

In this work, we consider three classes of approaches for generating adversarial examples: optimization-based approaches, fast gradient approaches, and fast gradient sign approaches. Each class has non-targeted and targeted versions respectively.

2.2.1 APPROACHES FOR GENERATING NON-TARGETED ADVERSARIAL EXAMPLES

Formally, given an image x with ground truth $y = f_\theta(x)$, searching for a non-targeted adversarial example can be modeled as searching for an instance $x^\star$ to satisfy the following constraints:

$$f_\theta(x^\star) \neq y \tag{1}$$
$$d(x, x^\star) \leq B \tag{2}$$

where $d(\cdot, \cdot)$ is a metric to quantify the distance between an original image and its adversarial counterpart, and B, called *distortion*, is an upper bound placed on this distance. Without loss of generality, we consider model f is composed of a network $J_\theta(x)$, which outputs the probability for each category, so that f outputs the category with the highest probability.

Optimization-based approach. One approach is to approximate the solution to the following optimization problem:

$$\mathbf{argmin}_{x^\star} \lambda d(x, x^\star) - \ell(\mathbf{1}_y, J_\theta(x^\star)) \tag{3}$$

where $\mathbf{1}_y$ is the one-hot encoding of the ground truth label y, ℓ is a loss function to measure the distance between the prediction and the ground truth, and λ is a constant to balance constraints (2) and (1), which is empirically determined. Here, loss function ℓ is used to approximate constraint (1), and its choice can affect the effectiveness of searching for an adversarial example. In this work, we choose $\ell(u, v) = \log(1 - u \cdot v)$, which is shown to be effective by Carlini & Wagner (2016).

Fast gradient sign (FGS). Goodfellow et al. (2014) proposed the fast gradient sign (FGS) method so that the gradient needs be computed only once to generate an adversarial example. FGS can be used to generate adversarial images to meet the L_∞ norm bound. Formally, non-targeted adversarial examples are constructed as

$$x^\star \leftarrow \text{clip}(x + B\mathbf{sgn}(\nabla_x \ell(\mathbf{1}_y, J_\theta(x))))$$

Here, $\text{clip}(x)$ is used to clip each dimension of x to the range of pixel values, i.e., $[0, 255]$ in this work. We make a slight variation to choose $\ell(u, v) = \log(1 - u \cdot v)$, which is the same as used in the optimization-based approach.

Fast gradient (FG). The fast gradient approach (FG) is similar to FGS, but instead of moving along the gradient sign direction, FG moves along the gradient direction. In particular, we have

$$x^\star \leftarrow \text{clip}(x + B\frac{\nabla_x \ell(\mathbf{1}_y, J_\theta(x))}{||\nabla_x \ell(\mathbf{1}_y, J_\theta(x))||}))$$

Here, we assume the distance metric in constraint (2), $d(x, x^\star) = ||x - x^\star||$ is a norm of $x - x^\star$. The term $\mathbf{sgn}(\nabla_x \ell)$ in FGS is replaced by $\frac{\nabla_x \ell}{||\nabla_x \ell||}$ to meet this distance constraint.

We call both FGS and FG *fast gradient-based approaches*.

2.2.2 APPROACHES FOR GENERATING TARGETED ADVERSARIAL EXAMPLES

A targeted adversarial image $x^\star$ is similar to a non-targeted one, but constraint (1) is replaced by

$$f_\theta(x^\star) = y^\star \tag{4}$$

where $y^\star$ is the target label given by the adversary. For the optimization-based approach, we approximate the solution by solving the following dual objective:

$$\mathbf{argmin}_{x^\star} \lambda d(x, x^\star) + \ell'(\mathbf{1}_{y^\star}, J_\theta(x^\star)) \tag{5}$$

In this work, we choose the standard cross entropy loss $\ell'(u, v) = -\sum_i u_i \log v_i$.

For FGS and FG, we construct adversarial examples as follows:

$$x^\star \leftarrow \text{clip}(x - B\mathbf{sgn}(\nabla_x \ell'(\mathbf{1}_{y^\star}, J_\theta(x)))) \quad \text{(FGS)}$$

$$x^\star \leftarrow \text{clip}(x - B\frac{\nabla_x \ell'(\mathbf{1}_{y^\star}, J_\theta(x))}{||\nabla_x \ell'(\mathbf{1}_{y^\star}, J_\theta(x))||}) \quad \text{(FG)}$$

where ℓ' is the same as the one used for the optimization-based approach.

2.3 EVALUATION METHODOLOGY

For the rest of the paper, we focus on examining the transferability among state-of-the-art models trained over ImageNet (Russakovsky et al. (2015)). In this section, we detail the models to be examined, the dataset to be evaluated, and the measurements to be used.

Models. We examine five networks, ResNet-50, ResNet-101, ResNet-152 (He et al. (2015))[1], GoogLeNet (Szegedy et al. (2014))[2], and VGG-16 (Simonyan & Zisserman (2014))[3]. We retrieve the pre-trained models for each network online. The performance of these models on the ILSVRC 2012 (Russakovsky et al. (2015)) validation set can be found in our online technical report: Liu et al. (2016). We choose these models to study the transferability between homogeneous architectures (i.e., ResNet models) and heterogeneous architectures.

Dataset. It is less meaningful to examine the transferability of an adversarial image between two models which cannot classify the original image correctly. Therefore, from the ILSVRC 2012 validation set, we randomly choose 100 images, which can be classified correctly by all five models in our examination. These 100 images form our test set. To perform targeted attacks, we manually choose a target label for each image, so that its semantics is far from the ground truth. The images and target labels in our evaluation can be found on website[4].

Measuring transferability. Given two models, we measure the non-targeted transferability by computing the percentage of the adversarial examples generated for one model that can be classified correctly for the other. We refer to this percentage as *accuracy*. A lower accuracy means better non-targeted transferability. We measure the targeted transferability by computing the percentage of the adversarial examples generated for one model that are classified as the target label by the other model. We refer to this percentage as *matching rate*. A higher matching rate means better targeted transferability. For clarity, the reported results are only based on top-1 accuracy. Top-5 accuracy's counterparts can be found in our online technical report: Liu et al. (2016).

[1] https://github.com/KaimingHe/deep-residual-networks
[2] https://github.com/BVLC/caffe/tree/master/models/bvlc_googlenet
[3] https://gist.github.com/ksimonyan/211839e770f7b538e2d8
[4] https://github.com/sunblaze-ucb/transferability-advdnn-pub

Distortion.   Besides transferability, another important factor is the distortion between adversarial images and the original ones. We measure the distortion by *root mean square deviation*, i.e., RMSD, which is computed as $d(x^\star, x) = \sqrt{\sum_i (x_i^\star - x_i)^2 / N}$, where $x^\star$ and x are the vector representations of an adversarial image and the original one respectively, N is the dimensionality of x and $x^\star$, and x_i denotes the pixel value of the i-th dimension of x, within range $[0, 255]$, and similar for $x_i^\star$.

3   NON-TARGETED ADVERSARIAL EXAMPLES

In this section, we examine different approaches for generating non-targeted adversarial images.

3.1   OPTIMIZATION-BASED APPROACH

To apply the optimization-based approach for a single model, we initialize $x^\star$ to be x and use Adam Optimizer (Kingma & Ba (2014)) to optimize Objective (3) . We find that we can tune the RMSD by adjusting the learning rate of Adam and λ. We find that, for each model, we can use a small learning rate to generate adversarial images with small RMSD, i.e. < 2, with any λ. In fact, we find that when initializing $x^\star$ with x, Adam Optimizer will search for an adversarial example around x, even when we set λ to be 0, i.e., not restricting the distance between $x^\star$ and x. Therefore, we set λ to be 0 for all experiments using optimization-based approaches throughout the paper. Although these adversarial examples with small distortions can successfully fool the target model, however, they cannot transfer well to other models (details can be found in our online technical report: Liu et al. (2016)).

We increase the learning rate to allow the optimization algorithm to search for adversarial images with larger distortion. In particular, we set the learning rate to be 4. We run Adam Optimizer for 100 iterations to generate the adversarial images. We observe that the loss converges after 100 iterations. An alternative optimization-based approach leading to similar results can be found in our online technical report: Liu et al. (2016).

Non-targeted adversarial examples transfer.   We generate non-targeted adversarial examples on one network, but evaluate them on another, and Table 1 Panel A presents the results. From the table, we can observe that

- The diagonal contains all 0 values. This says that all adversarial images generated for one model can mislead the same model.
- A large proportion of non-targeted adversarial images generated for one model using the optimization-based approach can transfer to another.
- Although the three ResNet models share similar architectures which differ only in the hyperparameters, adversarial examples generated against a ResNet model do not necessarily transfer to another ResNet model better than other non-ResNet models. For example, the adversarial examples generated for VGG-16 have lower accuracy on ResNet-50 than those generated for ResNet-152 or ResNet-101.

3.2   FAST GRADIENT-BASED APPROACHES

We then examine the effectiveness of fast gradient-based approaches. A good property of fast gradient-based approaches is that all generated adversarial examples lie in a 1-D subspace. Therefore, we can easily approximate the minimal distortion in this subspace of transferable adversarial examples between two models. In the following, we first control the RMSD to study fast gradient-based approaches' effectiveness. Second, we study the transferable minimal distortions of fast gradient-based approaches.

3.2.1   EFFECTIVENESS AND TRANSFERABILITY OF THE FAST GRADIENT-BASED APPROACHES

Since the distortion B and the RMSD of the generated adversarial images are highly correlated, we can choose this hyperparameter B to generate adversarial images with a given RMSD. In Table 1

	RMSD	ResNet-152	ResNet-101	ResNet-50	VGG-16	GoogLeNet
ResNet-152	22.83	0%	13%	18%	19%	11%
ResNet-101	23.81	19%	0%	21%	21%	12%
ResNet-50	22.86	23%	20%	0%	21%	18%
VGG-16	22.51	22%	17%	17%	0%	5%
GoogLeNet	22.58	39%	38%	34%	19%	0%

Panel A: Optimization-based approach

	RMSD	ResNet-152	ResNet-101	ResNet-50	VGG-16	GoogLeNet
ResNet-152	23.45	4%	13%	13%	20%	12%
ResNet-101	23.49	19%	4%	11%	23%	13%
ResNet-50	23.49	25%	19%	5%	25%	14%
VGG-16	23.73	20%	16%	15%	1%	7%
GoogLeNet	23.45	25%	25%	17%	19%	1%

Panel B: Fast gradient approach

Table 1: Transferability of non-targeted adversarial images generated between pairs of models. The first column indicates the average RMSD of all adversarial images generated for the model in the corresponding row. The cell (i, j) indicates the accuracy of the adversarial images generated for model i (row) evaluated over model j (column). Results of top-5 accuracy can be found in our online technical report: Liu et al. (2016).

Panel B, we generate adversarial images using FG such that the average RMSD is almost the same as those generated using the optimization-based approach. We observe that the diagonal values in the table are all positive, which means that FG cannot fully mislead the models. A potential reason is that, FG can be viewed as approximating the optimization, but is tailored for speed over accuracy.

On the other hand, the values of non-diagonal cells in the table, which correspond to the accuracies of adversarial images generated for one model but evaluated on another, are comparable with or less than their counterparts in the optimization-based approach. This shows that non-targeted adversarial examples generated by FG exhibit transferability as well.

We also evaluate FGS, but the transferability of the generated images is worse than the ones generated using either FG or optimization-based approaches. The results can be found in our online technical report: Liu et al. (2016). It shows that when RMSD is around 23, the accuracies of the adversarial images generated by FGS is greater than their counterparts for FG. We hypothesize the reason why transferability of FGS is worse to this fact.

3.2.2 ADVERSARIAL IMAGES WITH MINIMAL TRANSFERABLE RMSD

For an image x and two models M_1, M_2, we can approximate the minimal distortion B along a direction δ, such that $x_B = x + B\delta$ generated for M_1 is adversarial for both M_1 and M_2. Here δ is the direction, i.e., $\mathbf{sgn}(\nabla_x \ell)$ for FGS, and $\nabla_x \ell / ||\nabla_x \ell||$ for FG.

We refer to *the minimal transferable RMSD from M_1 to M_2 using FG (or FGS)* as the RMSD of a transferable adversarial example x_B with the minimal transferable distortion B from M_1 to M_2 using FG (or FGS). The minimal transferable RMSD can illustrate the tradeoff between distortion and transferability.

In the following, we approximate the minimal transferable RMSD through a linear search by sampling B every 0.1 step. We choose the linear-search method rather than binary-search method to determine the minimal transferable RMSD because the adversarial images generated from an original image may come from multiple intervals. The experiment can be found in our online technical report: Liu et al. (2016).

Minimal transferable RMSD using FG and FGS. Figure 1 plots the cumulative distribution function (CDF) of the minimal transferable RMSD from VGG-16 to ResNet-152 using non-targeted FG (Figure 1a) and FGS (Figure 1b). From the figures, we observe that both FG and FGS can find 100% transferable adversarial images with RMSD less than 80.91 and 86.56 respectively. Further,

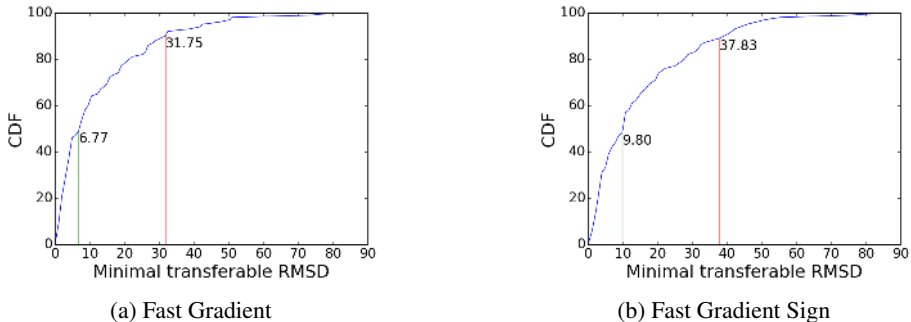(a) Fast Gradient

(b) Fast Gradient Sign

Figure 1: The CDF of the minimal transferable RMSD from VGG-16 to ResNet-152 using FG (a) and FGS (b). The green line labels the median minimal transferable RMSD, while the red line labels the minimal transferable RMSD to reach 90% percentage.

	RMSD	ResNet-152	ResNet-101	ResNet-50	VGG-16	GoogLeNet
ResNet-152	23.13	100%	2%	1%	1%	1%
ResNet-101	23.16	3%	100%	3%	2%	1%
ResNet-50	23.06	4%	2%	100%	1%	1%
VGG-16	23.59	2%	1%	2%	100%	1%
GoogLeNet	22.87	1%	1%	0%	1%	100%

Table 2: The matching rate of targeted adversarial images generated using the optimization-based approach. The first column indicates the average RMSD of the generated adversarial images. Cell (i, j) indicates that matching rate of the targeted adversarial images generated for model i (row) when evaluated on model j (column). The top-5 results can be found in our online technical report: Liu et al. (2016).

the FG method can generate transferable attacks with smaller RMSD than FGS. A potential reason is that while FGS minimizes the distortion's L_∞ norm, FG minimizes its L_2 norm, which is proportional to RMSD.

3.3 COMPARISON WITH RANDOM PERTURBATIONS

We also evaluate the test accuracy when we add a Gaussian noise to the 100 images in our test set. The concrete results can be found in our online technical report: Liu et al. (2016), where we show the conclusion that the "transferability" of this approach is significantly worse than either optimization-based approaches or fast gradient-based approaches.

4 TARGETED ADVERSARIAL EXAMPLES

In this section, we examine the transferability of targeted adversarial images. Table 2 presents the results for using optimization-based approach. We observe that (1) the prediction of targeted adversarial images can match the target labels when evaluated on the same model that is used to generate the adversarial examples; but (2) the targeted adversarial images can be rarely predicted as the target labels by a different model. We call the latter that *the target labels do not transfer*. Even when we increase the distortion, we still do not observe improvements on making target label transfer. Some results can be found in our online technical report: Liu et al. (2016). Even if we compute the matching rate based on top-5 accuracy, the highest matching rate is only 10%. The results can be found in our online technical report: Liu et al. (2016).

We also examine the targeted adversarial images generated by fast gradient-based approaches, and we observe that the target labels do not transfer as well. The results can be found in our online technical report: Liu et al. (2016). In fact, most targeted adversarial images cannot mislead the model, for which the adversarial images are generated, to predict the target labels, regardless of how large the distortion is used. We attribute it to the fact that the fast gradient-based approaches only

search for attacks in a 1-D subspace. In this subspace, the total possible predictions may contain a small subset of all labels, which usually does not contain the target label. In Section 6, we study decision boundaries regarding this issue.

We also evaluate the matching rate of images added with Gaussian noise, as described in Section 3.3. However, we observe that the matching rate of any of the 5 models is 0%. Therefore, we conclude that by adding Gaussian noise, the attacker cannot generate successful targeted adversarial examples at all, let alone targeted transferability.

5 ENSEMBLE-BASED APPROACHES

We hypothesize that if an adversarial image remains adversarial for multiple models, then it is more likely to transfer to other models as well. We develop techniques to generate adversarial images for multiple models. The basic idea is to generate adversarial images for *the ensemble of the models*. Formally, given k white-box models with softmax outputs being $J_1, ..., J_k$, an original image x, and its ground truth y, *the ensemble-based approach* solves the following optimization problem (for targeted attack):

$$\mathbf{argmin}_{x^\star} - \log \big((\sum_{i=1}^{k} \alpha_i J_i(x^\star)) \cdot \mathbf{1}_{y^\star} \big) + \lambda d(x, x^\star) \tag{6}$$

where $y^\star$ is the target label specified by the adversary, $\sum \alpha_i J_i(x^\star)$ is the ensemble model, and α_i are the ensemble weights, $\sum_{i=1}^{k} \alpha_i = 1$. Note that (6) is the targeted objective. The non-targeted counterpart can be derived similarly. In doing so, we hope the generated adversarial images remain adversarial for an additional black-box model J_{k+1}.

We evaluate the effectiveness of the ensemble-based approach. For each of the five models, we treat it as the black-box model to attack, and generate adversarial images for the ensemble of the rest four, which is considered as white-box. We evaluate the generated adversarial images over all five models. Throughout the rest of the paper, we refer to the approaches evaluated in Section 3 and 4 as the approaches using a single model, and to the ensemble-based approaches discussed in this section as the approaches using an ensemble model.

Optimization-based approach. We use Adam to optimize the objective (6) with equal ensemble weights across all models in the ensemble to generate targeted adversarial examples. In particular, we set the learning rate of Adam to be 8 for each model. In each iteration, we compute the Adam update for each model, sum up the four updates, and add the aggregation onto the image. We run 100 iterations of updates, and we observe that the loss converges after 100 iterations. By doing so, for the first time, we observe a large proportion of the targeted adversarial images whose target labels can transfer. The results are presented in Table 3. We observe that not all targeted adversarial images can be misclassified to the target labels by the models used in the ensemble. This suggests that while searching for an adversarial example for the ensemble model, there is no direct supervision to mislead any individual model in the ensemble to predict the target label. Further, from the diagonal numbers of the table, we observe that the transferability to ResNet models is better than to VGG-16 or GoogLeNet, when adversarial examples are generated against all models except the target model.

We also evaluate non-targeted adversarial images generated by the ensemble-based approach. We observe that the generated adversarial images have almost perfect transferability. We use the same procedure as for the targeted version, except the objective to generate the adversarial images. We evaluate the generated adversarial images over all models. The results are presented in Table 4. The generated adversarial images all have RMSDs around 17, which are lower than 22 to 23 of the optimization-based approach using a single model (See Table 1 for comparison). When the adversarial images are evaluated over models which are not used to generate the attack, the accuracy is no greater than 6%. For a reference, the corresponding accuracies for all approaches evaluated in Section 3 using one single model are at least 12%. Our experiments demonstrate that the ensemble-based approaches can generate almost perfectly transferable adversarial images.

Fast gradient-based approach. The results for non-targeted fast gradient-based approaches applied to the ensemble can be found in our online technical report: Liu et al. (2016). We observe that the diagonal values are not zero, which is the same as we observed in the results for FG and

	RMSD	ResNet-152	ResNet-101	ResNet-50	VGG-16	GoogLeNet
-ResNet-152	30.68	38%	76%	70%	97%	76%
-ResNet-101	30.76	75%	43%	69%	98%	73%
-ResNet-50	30.26	84%	81%	46%	99%	77%
-VGG-16	31.13	74%	78%	68%	24%	63%
-GoogLeNet	29.70	90%	87%	83%	99%	11%

Table 3: The matching rate of targeted adversarial images generated using the optimization-based approach. The first column indicates the average RMSD of the generated adversarial images. Cell (i, j) indicates that percentage of the targeted adversarial images generated for the ensemble of the four models except model i (row) is predicted as the target label by model j (column). In each row, the minus sign "−" indicates that the model of the row is not used when generating the attacks. Results of top-5 matching rate can be found in our online technical report: Liu et al. (2016).

	RMSD	ResNet-152	ResNet-101	ResNet-50	VGG-16	GoogLeNet
-ResNet-152	17.17	0%	0%	0%	0%	0%
-ResNet-101	17.25	0%	1%	0%	0%	0%
-ResNet-50	17.25	0%	0%	2%	0%	0%
-VGG-16	17.80	0%	0%	0%	6%	0%
-GoogLeNet	17.41	0%	0%	0%	0%	5%

Table 4: Accuracy of non-targeted adversarial images generated using the optimization-based approach. The first column indicates the average RMSD of the generated adversarial images. Cell (i, j) corresponds to the accuracy of the attack generated using four models except model i (row) when evaluated over model j (column). In each row, the minus sign "−" indicates that the model of the row is not used when generating the attacks. Results of top-5 accuracy can be found in our online technical report: Liu et al. (2016).

FGS applied to a single model. We hypothesize a potential reason is that the gradient directions of different models in the ensemble are orthogonal to each other, as we will illustrate in Section 6. In this case, the gradient direction of the ensemble is almost orthogonal to the one of each model in the ensemble. Therefore searching along this direction may require large distortion to reach adversarial examples.

For targeted adversarial examples generated using FG and FGS based on an ensemble model, their transferability is no better than the ones generated using a single model. The results can be found in our online technical report: Liu et al. (2016). We hypothesize the same reason to explain this: there are only few possible target labels in total in the 1-D subspace.

6 GEOMETRIC PROPERTIES OF DIFFERENT MODELS

In this section, we show some geometric properties of the models to try to better understand transferable adversarial examples. Prior works also try to understand the geometic properties of adversarial examples theoretically (Fawzi et al. (2016)) or empirically (Goodfellow et al. (2014)). In this work, we examine large models trained over a large dataset with 1000 labels, whose geometric properties are never examined before. This allows us to make new observations to better understand the models and their adversarial examples.

The gradient directions of different models in our evaluation are almost orthogonal to each other. We study whether the adversarial directions of different models align with each other. We calculate cosine value of the angle between gradient directions of different models, and the results can be found in our online technical report: Liu et al. (2016). We observe that all non-diagonal values are close to 0, which indicates that for most images, their gradient directions with respect to different models are orthogonal to each other.

Decision boundaries of the non-targeted approaches using a single model. We study the decision boundary of different models to understand why adversarial examples transfer. We choose two

Figure 2: The example image to study the decision boundary. Its ID in ILSVRC 2012 validation set is 49443, and its ground truth label is "anemone fish."
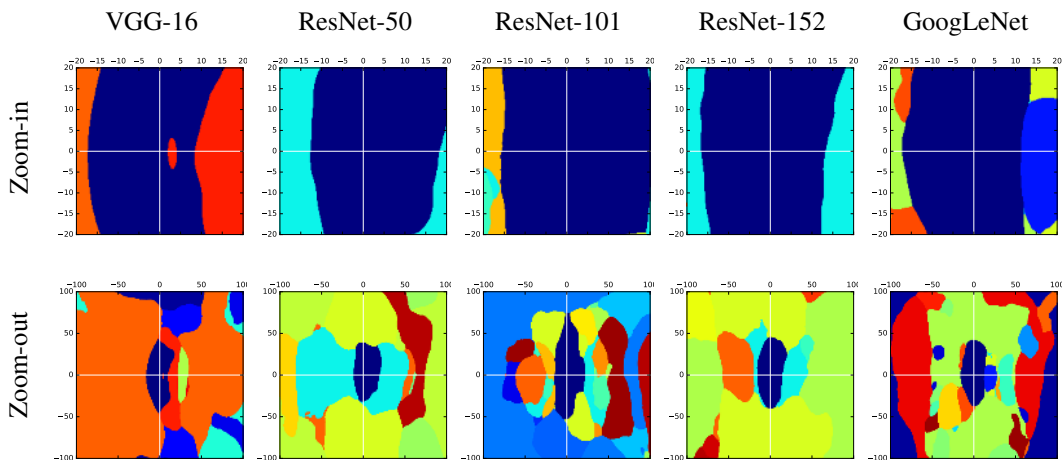

Figure 3: Decision regions of different models. We pick the same two directions for all plots: one is the gradient direction of VGG-16 (x-axis), and the other is a random orthogonal direction (y-axis). Each point in the span plane shows the predicted label of the image generated by adding a noise to the original image (e.g., the origin corresponds to the predicted label of the original image). The units of both axises are 1 pixel values. All sub-figure plots the regions on the span plane using the same color for the same label. The image is in Figure 2.

normalized orthogonal directions δ_1, δ_2, one being the gradient direction of VGG-16 and the other being randomly chosen. Each point (u, v) in this 2-D plane corresponds to the image $x + u\delta_1 + v\delta_2$, where x is the pixel value vector of the original image. For each model, we plot the label of the image corresponding to each point, and get Figure 3 using the image in Figure 2.

We can observe that for all models, the region that each model can predict the image correctly is limited to the central area. Also, along the gradient direction, the classifiers are soon misled. One interesting finding is that along this gradient direction, the first misclassified label for the three ResNet models (corresponding to the light green region) is the label "orange". A more detailed study can be found in our online technical report: Liu et al. (2016). When we look at the zoom-out figures, however, the labels of images that are far away from the original one are different for different models, even among ResNet models.

On the other hand, in Table 5, we show the total number of regions in each plane. In fact, for each plane, there are at most 21 different regions in all planes. Compared with the 1,000 total categories in ImageNet, this is only 2.1% of all categories. That means, for all other 97.9% labels, no targeted adversarial example exists in each plane. Such a phenomenon partially explains why fast gradient-based approaches can hardly find targeted adversarial images.

Further, in Figure 4, we draw the decision boundaries of all models on the same plane as described above. We can observe that

Model	VGG-16	ResNet-50	ResNet-101	ResNet-152	GoogLeNet
# of labels	10	9	21	10	21

Table 5: The number of all possible predicted labels for each model in the same plane described in Figure 3.
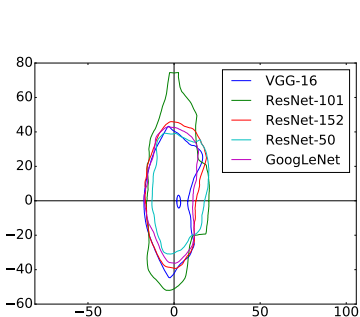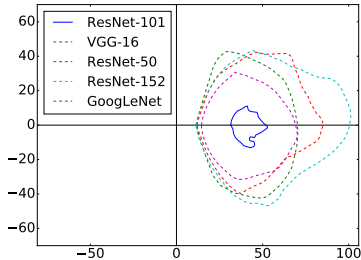

Figure 4: The decision boundary to separate the region within which all points are classified as the ground truth label (encircled by each closed curve) from others. The plane is the same one described in Figure 3. The origin of the coordinate plane corresponds to the original image. The units of both axises are 1 pixel values.

Figure 5: The decision boundary to separate the region within which all points are classified as the target label (encircled by each closed curve) from others. The plane is spanned by the targeted adversarial direction and a random orthogonal direction. The targeted adversarial direction is computed as the difference between the original image in Figure 2 and the adversarial image generated by the optimization-based approach for an ensemble. The ensemble contains all models except ResNet-101. The origin of the coordinate plane corresponds to the original image. The units of both axises are 1 pixel values.

- The boundaries align with each other very well. This partially explains why non-targeted adversarial images can transfer among models.

- The boundary diameters along the gradient direction is less than the ones along the random direction. A potential reason is that moving a variable along its gradient direction can change the loss function (i.e., the probability of the ground truth label) significantly. Therefore along the gradient direction it will take fewer steps to move out of the ground truth region than a random direction.

- An interesting finding is that even though we move left along the x-axis, which is equivalent to maximizing the ground truth's prediction probability, it also reaches the boundary much sooner than moving along a random direction. We attribute this to the non-linearity of the loss function: when the distortion is larger, the gradient direction also changes dramatically. In this case, moving along the original gradient direction no longer increases the probability to predict the ground truth label (details can be found in our online technical report: Liu et al. (2016)).

- As for VGG-16 model, there is a small hole within the region corresponding to the ground truth. This may partially explain why non-targeted adversarial images with small distortion exist, but do not transfer well. This hole does not exist in other models' decision planes. In this case, non-targeted adversarial images in this hole do not transfer.

Decision boundaries of the targeted ensemble-based approaches. In addition, we choose the targeted adversarial direction of the ensemble of all models except ResNet-101 and a random orthogonal direction, and we plot decision boundaries on the plane spanned by these two direction vectors in Figure 5. We observe that the regions of images, which are predicted as the target label, align well for the four models in the ensemble. However, for the model not used to generate the adversarial image, i.e., ResNet-101, it also has a non-empty region such that the prediction is successfully misled to the target label, although the area is much smaller. Meanwhile, the region within each closed curve of the models almost has the same center.

7 REAL WORLD EXAMPLE: ADVERSARIAL EXAMPLES FOR CLARIFAI.COM

Clarifai.com is a commercial company providing state-of-the-art image classification services. We have no knowledge about the dataset and types of models used behind Clarifai.com, except that we have black-box access to the services. The labels returned from Clarifai.com are also different from the categories in ILSVRC 2012. We submit all 100 original images to Clarifai.com and the returned labels are correct based on a subjective measure.

We also submit 400 adversarial images in total, where 200 of them are targeted adversarial examples, and the rest 200 are non-targeted ones. As for the 200 targeted adversarial images, 100 of them are generated using the optimization-based approach based on VGG-16 (the same ones evaluated in Table 2), and the rest 100 are generated using the optimization-based approach based on an ensemble of all models except ResNet-152 (the same ones evaluated in Table 3). The 200 non-targeted adversarial examples are generated similarly (the same ones evaluated in Table 1 and 4).

For non-targeted adversarial examples, we observe that for both the ones generated using VGG-16 and those generated using the ensemble, most of them can transfer to Clarifai.com.

More importantly, a large proportion of our targeted adversarial examples are misclassified by Clarifai.com as well. We observe that 57% of the targeted adversarial examples generated using VGG-16, and 76% of the ones generated using the ensemble can mislead Clarifai.com to predict labels irrelevant to the ground truth.

Further, our experiment shows that for targeted adversarial examples, 18% of those generated using the ensemble model can be predicted as labels close to the target label by Clarifai.com. The corresponding number for the targeted adversarial examples generated using VGG-16 is 2%. Considering that in the case of attacking Clarifai.com, the labels given by the target model are different from those given by our models, it is fairly surprising to see that when using the ensemble-based approach, there is still a considerable proportion of our targeted adversarial examples that can mislead this black-box model to make predictions semantically similar to our target labels. All these numbers are computed based on a subjective measure, and we include some examples in Table 6. More examples can be found in our online technical report: Liu et al. (2016).

original image	true label	Clarifai.com results of original image	target label	targeted adversarial example	Clarifai.com results of targeted adversarial example
	viaduct	bridge, sight, arch, river, sky	window screen		window, wall, old, decoration, design
	hip, rose hip, rosehip	fruit, fall, food, little, wildlife	stupa, tope		Buddha, gold, temple, celebration, artistic
	dogsled, dog sled, dog sleigh	group together, four, sledge, sled, enjoyment	hip, rose hip, rosehip		cherry, branch, fruit, food, season

	pug, pug-dog	pug, friendship, adorable, purebred, sit	sea lion		sea seal, ocean, head, sea, cute
	Old English sheep-dog, bobtail	poodle, retriever, loyalty, sit, two	abaya		veil, spirituality, religion, people, illustration
	maillot, tank suit	beach, woman, adult, wear, portrait	amphib-ian, amphibi-ous vehicle		transportation system, vehicle, man, print, retro
	patas, hussar monkey, Erythro-cebus patas	primate, monkey, safari, sit, looking	bee eater		ornithology, avian, beak, wing, feather

Table 6: Original images and adversarial images evaluated over Clarifai.com. For labels returned from Clarifai.com, we sort the labels firstly by rareness: how many times a label appears in the Clarifai.com results for all adversarial images and original images, and secondly by confidence. Only top 5 labels are provided.

8 CONCLUSION

In this work, we are the first to conduct an extensive study of the transferability of both non-targeted and targeted adversarial examples generated using different approaches over large models and a large scale dataset. Our results confirm that the transferability for non-targeted adversarial examples are prominent even for large models and a large scale dataset. On the other hand, we find that it is hard to use existing approaches to generate targeted adversarial examples whose target labels can transfer. We develop novel ensemble-based approaches, and demonstrate that they can generate transferable targeted adversarial examples with a high success rate. Meanwhile, these new approaches exhibit better performance on generating non-targeted transferable adversarial examples than previous work. We also show that both non-targeted and targeted adversarial examples generated using our new approaches can successfully attack Clarifai.com, which is a black-box image classification system. Furthermore, we study some geometric properties to better understand the transferable adversarial examples.

REFERENCES

Nicholas Carlini and David Wagner. Towards evaluating the robustness of neural networks. *arXiv preprint arXiv:1608.04644*, 2016.

Alhussein Fawzi, Seyed-Mohsen Moosavi-Dezfooli, and Pascal Frossard. Robustness of classifiers: from adversarial to random noise. In *Advances in Neural Information Processing Systems*, pp. 1624–1632, 2016.

Ian J Goodfellow, Jonathon Shlens, and Christian Szegedy. Explaining and harnessing adversarial examples. *arXiv preprint arXiv:1412.6572*, 2014.

Kaiming He, Xiangyu Zhang, Shaoqing Ren, and Jian Sun. Deep residual learning for image recognition. *arXiv preprint arXiv:1512.03385*, 2015.

Diederik P. Kingma and Jimmy Ba. Adam: A method for stochastic optimization. *CoRR*, abs/1412.6980, 2014. URL http://arxiv.org/abs/1412.6980.

Alex Krizhevsky and Geoffrey Hinton. Learning multiple layers of features from tiny images. 2009.

Yann LeCun, Léon Bottou, Yoshua Bengio, and Patrick Haffner. Gradient-based learning applied to document recognition. *Proceedings of the IEEE*, 86(11):2278–2324, 1998.

Yanpei Liu, Xinyun Chen, Chang Liu, and Dawn Song. Delving into transferable adversarial examples and black-box attacks. *arXiv preprint arXiv:1611.02770*, 2016.

Seyed-Mohsen Moosavi-Dezfooli, Alhussein Fawzi, Omar Fawzi, and Pascal Frossard. Universal adversarial perturbations. *arXiv preprint arXiv:1610.08401*, 2016.

Nicolas Papernot, Patrick McDaniel, and Ian Goodfellow. Transferability in machine learning: from phenomena to black-box attacks using adversarial samples. *arXiv preprint arXiv:1605.07277*, 2016a.

Nicolas Papernot, Patrick McDaniel, Ian Goodfellow, Somesh Jha, Z Berkay Celik, and Ananthram Swami. Practical black-box attacks against deep learning systems using adversarial examples. *arXiv preprint arXiv:1602.02697*, 2016b.

Olga Russakovsky, Jia Deng, Hao Su, Jonathan Krause, Sanjeev Satheesh, Sean Ma, Zhiheng Huang, Andrej Karpathy, Aditya Khosla, Michael Bernstein, Alexander C. Berg, and Li Fei-Fei. ImageNet Large Scale Visual Recognition Challenge. *International Journal of Computer Vision (IJCV)*, 115(3):211–252, 2015. doi: 10.1007/s11263-015-0816-y.

Karen Simonyan and Andrew Zisserman. Very deep convolutional networks for large-scale image recognition. *CoRR*, abs/1409.1556, 2014. URL http://arxiv.org/abs/1409.1556.

J. Stallkamp, M. Schlipsing, J. Salmen, and C. Igel. Man vs. computer: Benchmarking machine learning algorithms for traffic sign recognition. *Neural Networks*, (0):–, 2012. ISSN 0893-6080. doi: 10.1016/j.neunet.2012.02.016. URL http://www.sciencedirect.com/science/article/pii/S0893608012000457.

Christian Szegedy, Wojciech Zaremba, Ilya Sutskever, Joan Bruna, Dumitru Erhan, Ian Goodfellow, and Rob Fergus. Intriguing properties of neural networks. *arXiv preprint arXiv:1312.6199*, 2013.

Christian Szegedy, Wei Liu, Yangqing Jia, Pierre Sermanet, Scott E. Reed, Dragomir Anguelov, Dumitru Erhan, Vincent Vanhoucke, and Andrew Rabinovich. Going deeper with convolutions. *CoRR*, abs/1409.4842, 2014. URL http://arxiv.org/abs/1409.4842.